RAYLEIGH-BENARD CONVECTION INSTABILITY IN THE PRESENCE OF TEMPERATURE VARIATION AT THE LOWER WALL

by

Miloš M. JOVANOVIĆ*, Dragan S. ŽIVKOVIĆ, and Jelena D. NIKODIJEVIĆ

Faculty of Mechanical Engineering, University of Niš, Niš, Serbia

Original scientific paper/Review paper/Short paper
DOI: 10.2298/TSCI120505169J

This paper analyzes the 2-D viscous fluid flow between two parallel plates, where the lower plate is heated and the upper one is cooled. The temperature difference between the plates is gradually increased during a certain time period, and afterwards it is temporarily constant. The temperature distribution on the lower plate is not constant in x-direction, and there is longitudinal sinusoidal temperature variation imposed on the mean temperature. We investigate the wave number and amplitude influence of this variation on the stability of Rayleigh-Benard convective cells, by direct numerical simulation of 2-D Navier-Stokes and energy equation.

Key words: *direct numerical simulation of Navier-Stokes equation, Oberbeck--Boussinesq approximation, Rayleigh and Prandtl number, non-linear stability analysis*

Introduction

We study the Rayleigh-Benard stability problem for a fluid bound by bottom and top wall which are heated and cooled, respectively, and subject to the spatial temperature modulation at the lower horizontal wall. This modulation causes the convection rolls to set up immediately, although the value of Rayleigh number is beneath the critical one, we have so called forced Rayleigh-Benard convection (FRBC). The reason for this convection is the temperature gradient in vertical direction, which causes instable density stratification and subsequent the fluid motion. Rayleigh solved the problem of stability of the conducting state when a fluid in a gravitational field is bound from above and below with spatially constant but unequal wall temperatures. He obtained the critical value of a dimensionless parameter at which the flow starts. This parameter is called the Rayleigh number and it is the ratio between the driving buoyancy and the damping viscosity forces. Another parameter, that measures the relative strength of the non-linearity in the momentum equations *v. s.* that of heat equation, is the Prandtl number. They are defined in the following way:

$$\mathrm{Ra} = \frac{\mathrm{g}\,\beta(T_1 - T_2)d^3}{\alpha\nu}, \quad \mathrm{Pr} = \frac{\nu}{\alpha} \tag{1}$$

Here Ra is Rayleigh and Pr is Prandtl number, g is the gravitational acceleration, β – the thermal expansion coefficient, T_1 – the temperature of lower plate, T_2 – the temperature of upper plate, $d = 2H$ – the distance between the plates, ν – the kinematic viscosity, and

* Corresponding author; e-mail: jmilos@masfak.ni.ac.rs

α – the thermal diffusivity. In the above definition of the Rayleigh number, the fluid properties are calculated at mean temperature $T_m = (T_1 + T_2)/2$, because this is the best reference temperature. In our calculation T_1 is a temporal and x-direction variable function, and so is the Ra number, which is a non-dimensional parameter for the measure of the ratio of buoyancy and viscous diffusive forces.

The value of the critical Rayleigh number according to linear stability theory is $Ra_c = 1708$ at wavenumber $q_c = 3.117$. Beyond this value the fluid starts to move and forms the counter-rotating 2-D rolls, the cross-section of which is almost square. The cellular flow becomes considerably more complicated as Ra increases. The 2-D rolls break up in 3-D cells, which appear hexagonal in shape when viewed from above. With larger Ra numbers, the cells multiply, becoming oscillatory and finally turbulent. The flow becomes turbulent at $Ra = 10^4$ and Pr = 1, for water Pr = 7 we have $Ra = 10^5$, and for higher Pr numbers we have $Ra = 10^6$-10^7.

Most of the above is valid for small temperature differences between the plates when the so-called Oberbeck-Boussinesq approximation is valid. In this approximation, all fluid properties are considered constant except density, which is assumed to be a linear function of temperature:

$$\rho = \rho_2[1 - \beta(T - T_2)] \tag{2}$$

where ρ_2 is the fluid density at the upper plate, and T – the fluid temperature between the walls. One of the first papers that analyzed the Rayleigh-Benard flow with variable viscosity is that of Tipelkirch [1]. Probably the first work where the Rayleigh-Benard flow was treated through assuming all fluid properties as a function of temperature was that of Paolucci [2]. Thereafter, many works have appeared treating Rayleigh-Benard flow with temperature dependant viscosity [3-7]. Their working fluid was air with dynamic viscosity and thermal conductivity following the Sutherland law. Then it was followed by the work of Frohlich *et al.* [8] and Severin *et al.* [9], which is the work on Rayleigh-Benard convection considering all fluid properties variable. Severin *et al.* [9] calculated the critical Reynolds number by using the method of asymptotic expansions and their results were valid only for small heat transfer rates. It is also of interest the most recent work of Nourollahi *et al.* [10], which is the work on entropy generation and Nusselt number in Rayleigh-Benard flow for six different values of the orientation angle, as well as the work of Gupta *et al.* [11] that analyses the very complex problem of the thermal instability of compressible electrically conducting Walters (model B') fluid layer permeated with suspended fluid particles.

In the present work we consider the fluid flow for the Rayleigh number below the critical value against the wavenumber $q = q_m = 3.7$ close to critical one ($q_c = 3.117$). The numerical simulation of 2-D Navier-Stokes equation in vorticity-streamfunction form is carried out for temperature-dependent thermophysical properties. In this cases we have the spatial temperature modulation at the lower wall, where δ_m is the amplitude and q_m is the wavenumber of temperature modulation around some average value at the lower plate.

The mathematical model

At Rayleigh-Benard convection we can use three different approaches: Oberbeck--Boussinesq approximation, low Mach number approximation, and compressible Navier--Stokes equations. The non-dimensional Oberbeck-Boussinesq equation system in the vorticity-streamfunction form reads:

$$\frac{\partial \omega}{\partial t} + (\vec{\mathrm{v}} \cdot \nabla)\omega = \mathrm{Pr}\Delta\omega + \mathrm{PrRa}\frac{\partial \theta}{\partial x} \tag{3}$$

$$\omega + \Delta\psi = 0 \tag{4}$$

$$\frac{\partial \theta}{\partial t} + (\vec{\mathrm{v}} \cdot \nabla)\theta = \Delta\theta \tag{5}$$

The boundary conditions are the following

$$\theta = 0, \quad \psi = 0, \quad \partial\psi/\partial y = 0, \text{ at } y = 1, \tag{6}$$

$$\theta = 1, \quad \psi = 0, \quad \partial\psi/\partial y = 0, \text{ at } y = -1, \tag{7}$$

$$D = \left\{ (x, y) \in \mathrm{R} \,\middle|\, 0 \le x \le 2\pi, -1 \le y \le 1 \right\}. \tag{8}$$

Here ω is the dimensionless vorticity of the fluid, ψ – the dimensionless streamfunction, θ – the dimensionless temperature, and $\vec{\mathrm{v}}$ – the dimensionless velocity vector, which are functions of dimensionless co-ordinates *x*, *y*, and dimensionless time *t*. The non-dimensional temperature θ is defined as:

$$\theta = \frac{T - T_2}{T_1 - T_2} \tag{9}$$

We have two boundary conditions for streamfunction and none for the vorticity. The problem is solved by the influence matrix method [12, 13], so that the first two eqs. (3) and (4) can be solved simultaneously, and the numerical method is described in detail [14]. We describe here only the numerical method used for energy equation.

Solution procedure

The above set of equations should be solved simultaneously in time, so we describe the procedure only for the energy equation. For the solution of the described problem we use the Fourier-Chebyshev pseudospectral method, with the Fourier-Galerkin method for approximation in homogeneous x-direction and Chebyshev collocation method for non-homogenous y-direction. The eq. (5) in a developed form is:

$$\frac{\partial \theta}{\partial t} + u\frac{\partial \theta}{\partial x} + v\frac{\partial \theta}{\partial y} = \frac{\partial^2 \theta}{\partial x^2} + \frac{\partial^2 \theta}{\partial y^2} + S \tag{10}$$

Here *S* is the source term, which in our case is zero. Fourier approximation in streamwise direction can be expressed by trigonometric polynomials in the exponential form:

$$\theta(x, y, t) = \sum_{k=-K}^{K} \hat{\theta}_k(y, t)\mathrm{e}^{\boldsymbol{i}kx}, \qquad S(x, y, t) = \sum_{k=-K}^{K} \hat{s}_k(y, t)\mathrm{e}^{\boldsymbol{i}kx} \tag{11}$$

$$v(x, y, t) = \sum_{k=-K}^{K} \hat{v}_k(y, t)\mathrm{e}^{\boldsymbol{i}kx}, \qquad u(x, y, t) = \sum_{k=-K}^{K} \hat{u}_k(y, t)\mathrm{e}^{\boldsymbol{i}kx} \tag{12}$$

$$u\frac{\partial\theta}{\partial x}(x,y,t)=\sum_{k=-K}^{K}\left(u\frac{\partial\theta}{\partial x}\right)_k(y,t)\,\mathrm{e}^{\underline{i}kx}=\sum_{k=-K}^{K}B_{1,k}(y,t)\,\mathrm{e}^{\underline{i}kx} \tag{13}$$

$$v\frac{\partial\theta}{\partial y}(x,y,t)=\sum_{k=-K}^{K}\left(v\frac{\partial\theta}{\partial y}\right)_k(y,t)\,\mathrm{e}^{\underline{i}kx}=\sum_{k=-K}^{K}B_{2,k}(y,t)\,\mathrm{e}^{\underline{i}kx} \tag{14}$$

Here $\hat{s}(t,y)$, $\hat{u}(t,y)$, $\hat{B}_{1,k}(t,y)$, and $\hat{B}_{2,k}(t,y)$ designate Fourier coefficients in the exponential form of trigonometric polynomials in (11)-(14) and $\underline{i}$ is the imaginary unit. After substitution (11), (12), (13), and (14) in (10) and differentiation we have:

$$\sum_{k=-K}^{K}\frac{\partial\hat{\theta}_k}{\partial t}(y,t)\mathrm{e}^{\underline{i}kx}+\sum_{k=-K}^{K}\hat{B}_{1,k}(y,t)\,\mathrm{e}^{\underline{i}kx}+\sum_{k=-K}^{K}\hat{B}_{2,k}(y,t)\mathrm{e}^{\underline{i}kx}=$$

$$=(\underline{i}k)^2\sum_{k=-K}^{K}\hat{\theta}_k(y,t)\mathrm{e}^{\underline{i}kx}+\sum_{k=-K}^{K}\frac{\partial^2\hat{\theta}_k}{\partial y^2}(y,t)\mathrm{e}^{\underline{i}kx}+\sum_{k=-K}^{K}\hat{s}_k(y,t)\mathrm{e}^{\underline{i}kx} \tag{15}$$

If we apply the Galerkin method and the orthogonality condition then our system of equations is reduced to:

$$\frac{\partial\hat{\theta}_k}{\partial t}(y,t)+\hat{B}_{1,k}(y,t)+\hat{B}_{2,k}(y,t)+k^2\hat{\theta}_k(y,t)=\frac{\partial^2\hat{\theta}_k}{\partial y^2}(y,t)+\hat{s}_k(y,t),$$
$$l=k=-N_x/2,...,N_x/2 \tag{16}$$

For approximation in y-direction we use the Chebyshev-collocation method in the following way:

$$\frac{\partial\hat{\theta}_k}{\partial t}(y_j,t)+\hat{B}_{1,k}(y_j,t)+\hat{B}_{2,k}(y_j,t)+k^2\hat{\theta}_k(y_j,t)=\sum_{l=0}^{N_y}d_{j,l}^{(2)}\hat{\theta}_k(y_l,t)+\hat{s}_k(y_j,t),$$

$$k=-N_x/2,...,N_x/2,\quad y_j=\cos\frac{\pi j}{N_y},\quad j=1,...,N_y-1 \tag{17}$$

where $d_{j,l}^{(2)}$ are elements of Chebyshev differentiation matrix [15]. The boundary points $j = 0$ and $j = N_y$ are not included in the above system of equations. If we designate:

$$\hat{B}_k(y_j,t)=\hat{B}_{1,k}(y_j,t)+\hat{B}_{2,k}(y_j,t) \tag{18}$$

for discretization in time, the second order finite difference method in the generalized form yields:

$$\frac{(1+\varepsilon)\hat{\theta}_k^{n+1}(y_j)-2\varepsilon\hat{\theta}_k^{n}(y_j)-(1-\varepsilon)\hat{\theta}_k^{n-1}(y_j)}{2\Delta t}+$$
$$+\left[\gamma_1\hat{B}_k^{n+1}(y_j)+\gamma_2\hat{B}_k^{n}(y_j)+(1-\gamma_1-\gamma_2)\hat{B}_k^{n-1}(y_j)\right]+$$
$$+k^2\left[\alpha\,\hat{\theta}_k^{n+1}(y_j)+(1-\alpha)\,\hat{\theta}_k^{n}(y_j)\right]= \tag{19}$$
$$=\sum_{l=0}^{N_y} d_{j,l}^{(2)}\left[\alpha\,\hat{\theta}_k^{n+1}(y_l)+(1-\alpha)\,\hat{\theta}_k^{n}(y_l)\right]+\alpha\,\hat{s}_k^{n+1}(y_j)+(1-\alpha)\hat{s}_k^{n}(y_j)$$
$$k=0,...,N_x/2,\quad y_j=\cos\frac{\pi j}{N_y},\ j=1,...,N_y-1,\ t_n=n\Delta t;\ n=0,1,...,N_t$$

We use the semi-implicit Adams-Bashworth/backward differentiation method where we have:

$$\varepsilon=2,\quad \gamma_1=0,\quad \gamma_2=2,\quad \alpha_1=1,\quad \alpha_2=0,\quad i.\,e.\quad \alpha_1=\alpha,\quad \alpha_2=1-\alpha \tag{20}$$

The values $\hat{\theta}_k^{n+1}$ have to be calculated for each wave number $k = 0,\ldots,N_x/2$, and each collocation point $y_j=\cos(\pi j/N_y)$, $j=0,1,...,N_y$. The generalized form of the set of eqs. (19) can be solved for $\gamma_1 = 0$, $\gamma_2 = 2$ in the following way:

$$\left[\frac{(1+\varepsilon)}{2\Delta t}+k^2\alpha-\alpha\sum_{l=0}^{N_y}d_{j,l}^{(2)}\right]\hat{\theta}_k^{n+1}(y_j)+\left[\frac{-2\varepsilon}{2\Delta t}+k^2(1-\alpha)-(1-\alpha)\sum_{l=0}^{N_y}d_{j,l}^{(2)}\right]\hat{\theta}_k^{n}(y_j)$$
$$-\frac{(1-\varepsilon)}{2\Delta t}\hat{\theta}_k^{n-1}(y_j)=\alpha\,\hat{s}_k^{n+1}(y_j)+(1-\alpha)\hat{s}_k^{n}(y_j)-\left[2\hat{B}_k^{n}(y_j)-\hat{B}_k^{n-1}(y_j)\right] \tag{21}$$
$$k=-N_x/2,...,N_x/2,\quad y_j=\cos\frac{\pi j}{N_y},\quad j=1,...,N_y-1,\quad t_n=n\Delta t;\qquad n=0,1,...,N_t$$

If we introduce the following matrices:

$$\mathrm{I}_1=\left[\delta_{i,j}\right]_{j=0,...,N_y}^{i=1,...,N_x-1},\qquad \mathrm{D}_4=\left[d_{i,j}^{(2)}\right]_{j=0,...,N_y}^{i=1,...,N_x-1} \tag{22}$$

and scalars

$$\sigma_1=\frac{1+\varepsilon}{2\Delta t}+k^2\alpha,\qquad \sigma_0=\frac{-\varepsilon}{\Delta t}+k^2(1-\alpha),\qquad \sigma_{-1}=-\frac{1-\varepsilon}{2\Delta t} \tag{23}$$

then we obtain the above system of eq. (21) in the form:

$$\left[\sigma_1\mathrm{I}_1-\alpha\mathrm{D}_4\right]\hat{\theta}_k^{n+1}+\left[\sigma_0\mathrm{I}_1-(1-\alpha)\mathrm{D}_4\right]\hat{\theta}_k^{n}-\sigma_{-1}\mathrm{I}_1\hat{\theta}_k^{n-1}=\alpha\mathrm{I}_1\hat{s}_k^{n+1}+(1-\alpha)\mathrm{I}_1\hat{s}_k^{n}-2\hat{B}_k^{n}+\hat{B}_k^{n-1},$$
$$k=-N_x/2,...,N_x/2,\qquad t_n=n\Delta t;\qquad n=0,1,...,N_t \tag{24}$$

where

$$\hat{\theta}_k^{n}=[\hat{\theta}_k^{n}(y_0),...,\hat{\theta}_k^{n}(y_{N_y})]^T,\quad \hat{s}_k^{n}=[\hat{s}_k^{n}(y_0),...,\hat{s}_k^{n}(y_{N_y})]^T,\quad \hat{B}_k^{n}=[\hat{B}_k^{n}(y_0),...,\hat{B}_k^{n}(y_{N_y})]^T \tag{25}$$

If we introduce the notation:

$$\mathrm{B}_1 = \left[\sigma_1 \mathrm{I}_1 - \alpha \mathrm{D}_4\right], \quad \mathrm{B}_0 = \left[\sigma_0 \mathrm{I}_1 - (1-\alpha)\mathrm{D}_4\right], \quad \mathrm{B}_{-1} = -\sigma_{-1}\mathrm{I}_1 \tag{26}$$

we finally obtain this matrix equation:

$$\begin{gathered} \mathrm{B}_1 \hat{\theta}_k^{n+1} + \mathrm{B}_0 \hat{\theta}_k^{n} + \mathrm{B}_{-1} \hat{\theta}_k^{n-1} = \alpha \mathrm{I}_1 \hat{s}_k^{n+1} + (1-\alpha)\mathrm{I}_1 \hat{s}_k^{n} - 2\widehat{B}_k^{n} + \widehat{B}_k^{n-1}, \\ k = 0,...,N_x/2, \quad t_n = n\Delta t, \quad n = 0,1,...,N_t \end{gathered} \tag{27}$$

This system of equations should be supplemented by boundary conditions. The horizontal walls are assumed to be isothermal with temperatures $\theta_{\mathrm{hot}} = 1$ and $\theta_{\mathrm{cold}} = 0$ (at classical RBC, in our FRBC case $\theta_{\mathrm{hot}} = \left(1 + \delta_m \sin q_m x + \delta_m \cos q_m x\right)\sin \omega t$ at the bottom and top walls, respectively:

$$\theta_{\mathrm{cold}}\left(y = 1\right) = \frac{T_2 - T_2}{T_1 - T_2} = 0; \qquad \theta_{\mathrm{hot}}\left(y = -1\right) = \frac{T_1 - T_2}{T_1 - T_2} = 1 \tag{28}$$

The generalized Robin boundary conditions have the form

$$\alpha_+ \theta\left(y_0, t\right) + \beta_+ \frac{\partial \theta}{\partial y}\left(y_0, t\right) = g_+(t), \qquad \alpha_- \theta\left(y_N, t\right) + \beta_- \frac{\partial \theta}{\partial y}\left(y_N, t\right) = g_-(t) \tag{29}$$

Here $\alpha_-, \alpha_+, \beta_+$, and β_- are constants and can have the value 1 or 0, depending on the type of boundary conditions (Robin, Dirichlet or Neumann boundary condition). Time variables g_+, and g_- are prescribed boundary conditions for temperature and/or heat flux on upper and lower plate. After the implementation of Chebyshev collocation method we have:

$$\alpha_+ \theta\left(y_0, t\right) + \beta_+ \sum_{j=0}^{j=N} d_{0.j}^{(1)} \theta\left(y_j, t\right) = g_+(t), \qquad \alpha_- \theta\left(y_N, t\right) + \beta_- \sum_{j=0}^{j=N} d_{N.j}^{(1)} \theta\left(y_j, t\right) = g_-(t) \tag{30}$$

In these equation N is the number of collocation point in y-direction. Boundary conditions on the upper and lower plate can be represented in this way:

$$g_+\left(x, 1, t\right) = \sum_{k=-K}^{K} \hat{g}_{+,k}\left(y, t\right) e^{\boldsymbol{i} k x}, \quad g_-\left(x, -1, t\right) = \sum_{k=-K}^{K} \hat{g}_{-,k}\left(y, t\right) \mathrm{e}^{\boldsymbol{i} k x} \tag{31}$$

If we multiply by $\mathrm{e}^{\boldsymbol{i} l x}$ and implement the orthogonality condition we get:

$$\begin{aligned} \alpha_+ \hat{\theta}_k\left(y_0, t\right) + \beta_+ \sum_{j=0}^{N} d_{0.j}^{(1)} \hat{\theta}_k\left(y_j, t\right) &= \hat{g}_{+,k}\left(t\right) \\ \alpha_- \hat{\theta}_k\left(y_N, t\right) + \beta_- \sum_{j=0}^{N} d_{N.j}^{(1)} \hat{\theta}_k\left(y_j, t\right) &= \hat{g}_{-,k}\left(t\right) \end{aligned} \tag{32}$$

In our case we have:

$$\begin{bmatrix} \alpha_+ + \beta_+ d_{0,0}^{(1)} & \beta_+ d_{0,1}^{(1)} & \beta_+ d_{0,2}^{(1)} & \cdots & \beta_+ d_{0,N}^{(1)} \\ \beta_- d_{N,0}^{(1)} & \beta_- d_{N,1}^{(1)} & \beta_- d_{N,2}^{(1)} & \cdots & \beta_- d_{N,2}^{(1)} + \alpha_- \end{bmatrix} \begin{Bmatrix} \hat{\theta}_k\left(y_0\right) \\ \vdots \\ \hat{\theta}_k\left(y_N\right) \end{Bmatrix}^{n+1} = \begin{bmatrix} \hat{g}_{+,k} \\ \hat{g}_{-,k} \end{bmatrix}^{n+1} \tag{33}$$

$$\mathrm{D}_6 = \begin{bmatrix} \alpha_+ + \beta_+ d_{0,0}^{(1)} & \beta_+ d_{0,1}^{(1)} & \beta_+ d_{0,2}^{(1)} & \cdots & \beta_+ d_{0,N}^{(1)} \\ \beta_- d_{N,0}^{(1)} & \beta_- d_{N,1}^{(1)} & \beta_- d_{N,2}^{(1)} & \cdots & \beta_- d_{N,2}^{(1)} + \alpha_- \end{bmatrix}, \quad \hat{g}_1^{n+1} = \begin{bmatrix} \hat{g}_{+,k} \\ \hat{g}_{-,k} \end{bmatrix}^{n+1}$$

$$\begin{gathered} \mathrm{D}_6 \hat{\theta}_k^{n+1} = \hat{g}_k^{n+1}; \quad k = 0,...,N_x/2, \\ t_n = n\Delta t; \quad n = 0,1,...,N_t \end{gathered} \tag{34}$$

The system of eqs. (27) and (34) can be solved by direct methods:

$$\begin{gathered} \mathrm{B}_1 \hat{\theta}_k^{n+1} = \alpha \mathrm{I}_1 \hat{s}_k^{n+1} + (1-\alpha)\mathrm{I}_1 \hat{s}_k^n - 2\hat{B}_k^n + \hat{B}_k^{n-1} - \mathrm{B}_0 \hat{\theta}_k^n - \mathrm{B}_{-1} \hat{\theta}_k^{n-1} = \hat{h}_k^{n+1}, \\ \mathrm{D}_6 \hat{\theta}_k^{n+1} = \hat{g}_k^{n+1}; \quad k = 0,...,N_x/2, \quad t_n = n\Delta t; \quad n = 0,1,...,N_t \end{gathered} \tag{35}$$

If we introduce the following notation:

$$\mathrm{A} = \begin{bmatrix} \mathrm{B}_1 \\ \mathrm{D}_6 \end{bmatrix}, \qquad \hat{f}_k^{n+1} = \begin{bmatrix} \hat{h}_k^{n+1} \\ \hat{g}_k^{n+1} \end{bmatrix} \tag{36}$$

the system is reduced to:

$$\mathrm{A}\hat{\theta}_k^{n+1} = \hat{f}_k^{n+1}, \quad k = 0,...,N_x/2, \quad n = 0,1,...,N_t \tag{37}$$

This system of eq. (37) should be solved in the given time step prior to the solution of momentum equation in the vorticity-streamfunction form (3) and definition of vorticity in terms of streamfunction (4). The calculated values of θ^{n+1} obtained as a solution of (37) should be used in eq. (3). The system of eqs. (3), (4), and (37) is solved for each time step $n = 0, 1, \ldots, N_t$ for all wave numbers $k = 0, 1, \ldots, N_x/2$.

Initial and boundary conditions and simulation results

We consider the initial condition for our simulation for the case of forced Rayleigh--Benard convection with temperature modulation on the lower wall:

$$\begin{gathered} \omega(x,y,t=0) = 0, \quad \psi(x,y,0) = 0, \quad \theta(x,y,0) = 0, \\ \text{for } \forall (x,y) \in D = \{(x,y) \in \mathrm{R} \mid 0 \le x \le 2\pi, -1 \le y \le 1\} \end{gathered} \tag{38}$$

The temperature at the lower plate is raised gradually according to the following law:

$$\begin{aligned} \theta(x,y=-1,t) &= (1 + \delta_\mathrm{m} \sin q_\mathrm{m} x + \delta_\mathrm{m} \cos q_\mathrm{m} x)\sin \omega t, && 0 \le t \le \pi/2\omega \\ \theta(x,y=-1,t) &= (1 + \delta_\mathrm{m} \sin q_\mathrm{m} x + \delta_\mathrm{m} \cos q_\mathrm{m} x), && \pi/2\omega < t \end{aligned} \tag{39}$$

The temperature at the lower wall is not constant in x-direction, it depends on modulation wavenumber q_m, amplitude δ_m and frequency ω. Rayleigh number Ra measures the average temperature gradient, while the additional spatial modulation is characterized by small amplitude δ_m and wavenumber q_m. In the absence of forcing ($\delta_\mathrm{m} = 0$), convection rolls with wavenumber q_c, bifurcate only for Ra above the critical Rayleigh number Ra_c.

In contrast, for $\delta_\mathrm{m} \neq 0$, convection is unavoidable for any finite Ra; in the simplest case in the form of "forced rolls" with the wave vector q_m. The main goal of the present work

is to provide a direct numerical simulation of rolls and their stability in presence of forcing with small amplitude $\delta_m = O(0.01)$ and in the ratio $q_m/q_c = 1.2$. The stability of the forced rolls strongly depends on ratio q_m/q_c. It is very important to emphasize that our Ra number vary temporally and spatially, since temperature at the lower wall is described by eq. (39), and temperature difference $T_1 - T_2$ in eq. (1) varies with time t and x-co-ordinate. Our idea is to show the evolution of streamfunction, vorticity, velocity in the transition period $0 \le t \le \pi$, for frequency $\omega = 1$. The values we have chosen are subcritical values Ra = 1000, $q_m = 3.7$ according to linear stability analysis, for Pr = 7, $\Delta t = \pi/300$, $\delta_m = 0.01$, number of Fourier modes K = 96, number of nodes $N_x = 192$, number of Chebyshev collocation points $N_y = 192$.

The results of direct numerical simulation

It is well known that in a large layer of heated fluid, convection occurs as a steady pattern of 2-D rolls. The 2-D convection rolls and stability properties were investigated in detail in [16] and [17]. For heated layer corresponding to $Ra > Ra_c$ the stable roll patterns occur only within a band of wavenumber centered approximately about the critical wavenumber q_c.

In this section we present the results of the numerical simulation obtained by our 2-D pseudo-spectral code for Navier-Stokes equation in streamfunction-vorticity formulation and energy equation, with the initial and boundary conditions described above. The vorticity distribution for six instants of non-dimensional time $t = \pi/6$, $\pi/3$, $\pi/2$, $2\pi/3$, $5\pi/6$, and π is shown in fig. 1. Since we have chosen $q_m = 3.7$, such number of the pair of rolls can be seen at $t = \pi/6$ at the lower wall. The maximal and minimal values of vorticity at the lower wall are slightly lower than –2 and above 2. In the next instant of time $t = \pi/3$ we can see the increase in the vorticity intensity, where it attains the values in the range from –19 to 20, and the distribution remains almost unperturbed. In the next instant of time $t = \pi/2$ we can see slight vorticity distribution deformation, and the jump in the range of the values from –50 to 50. This is the instant of time when the temperature at the lower wall has attained its final value, but with its modulation in x-direction. At $t = 2\pi/3$ the convective terms in energy equation start to transport vorticity in upwards direction and extreme values of vorticity increase further $-90 \le \omega \le 90$ although the temperature at the lower wall is temporarily constant now, but with modulation in x-direction. At $t = 5\pi/6$ we can see that the vorticity rolls are pushed upwards and that the concentration of vorticity appears at the upper wall, whereby the range of vorticity is now $-105 \le \omega \le 120$. Finally at $t = \pi$, the vorticity circulation is established, forced by buoyancy effect, and the positive and negative vortexes at the upper wall are much more noticeable than before, although there is no temperature modulation on upper plate, that is the source of ω.

The results of the numerical simulation for streamfunction are given in fig. 2. We can see that the range of values is increased not only for the time period when the temperature at the lower wall is increased ($t \le \pi/2$), but also when the temperature attains its constant value ($\pi/2 < t$). The spatial distribution of the instantaneous streamlines is unaltered in time period $0 \le t \le \pi/2$, but afterwards $\pi/2 \le t \le \pi$ convective terms attain values that significantly change the intensity and distribution.

The instantaneous streamlines are shown with constant colors intensity in fig. 2, where we can see more than three ($q_m = 3.7$) pair of positive and negative streamfunction areas in the vicinity of bottom wall with equal size and spatial distribution in x-direction for time period ($t \le \pi/2$), but as time elapses we can notice their intensity increase, which can be seen on the color bars on right hand side. In the period of time $t > \pi/2$, we can see that their intensity still increase but their spatial distribution is not even and their size is not equal.

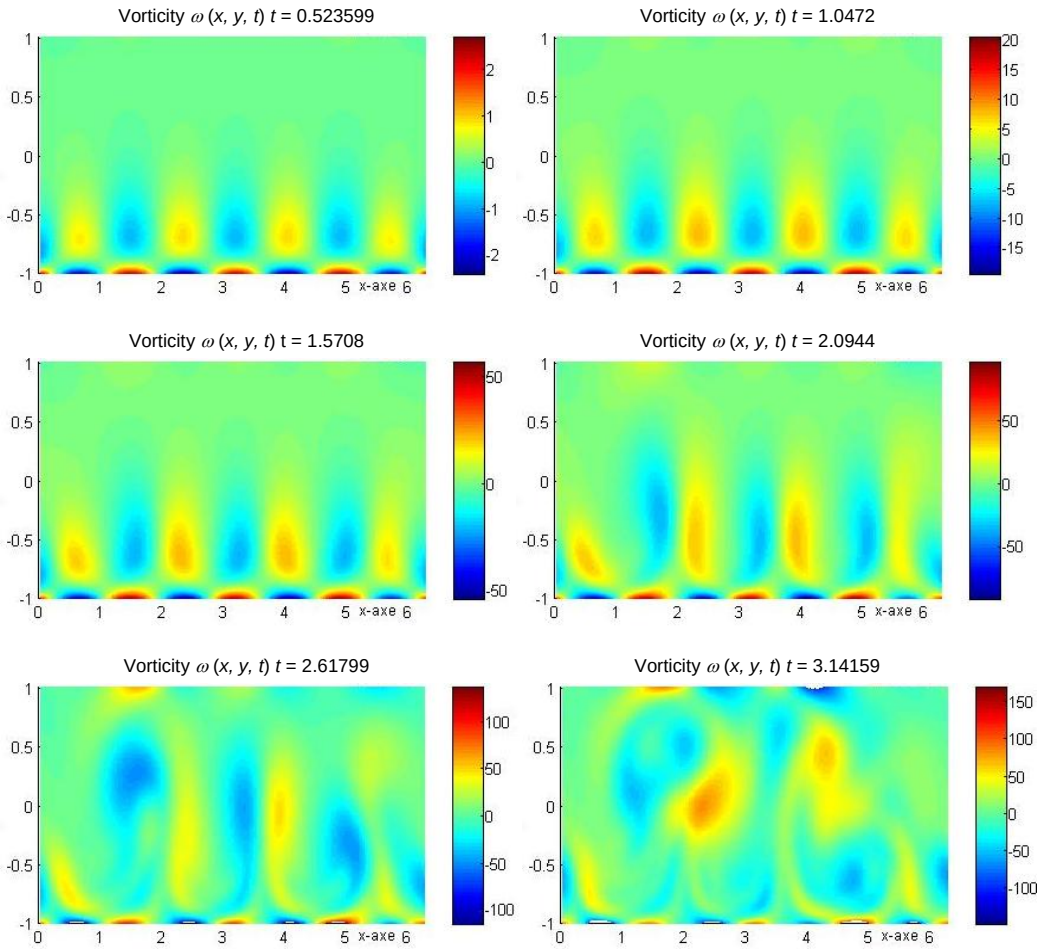

Figure 1. Non-dimensional vorticity evolution in forced Rayleigh-Benard convection

At $t = \pi$ we see the different streamfunction distribution in the middle of the channel, the area of extreme values of streamfunction lift up from the lower wall, so we have now two positive and one negative streamlines area instead of seven we had at $t = \pi/6$, what is the consequence of non-linear instability.

The results of numerical simulation for velocity in x-direction are given in fig. 3. The *u*-velocity keeps its form in time period $0 \le t \le \pi/2$, but afterwards $\pi/2 \le t \le \pi$ buoyancy effect becomes significant, and convective terms attain values that significantly change the intensity and distribution of *u*-velocity. In time period $\pi/2 \le t \le \pi$ distribution pattern changes and becomes partly disordered. The range of values increases although the temperature at the lower wall reaches its constant value at instant of time $t = \pi/2$ and afterward remains constant. The fluid heating through the lower wall and fluid cooling through the upper wall is not in balance so the increase in kinetic and thermal energy in the fluid flow is remarkable. The range of values in $t = 2\pi/3$ is $-5 \le u \le 5$, in $t = 5\pi/6$ is $-6.5 \le u \le 8.25$, and in $t = \pi$ is $-11 \le u \le 10.5$, and the position of the extreme values is pushed from the lower wall toward the middle of the channel.

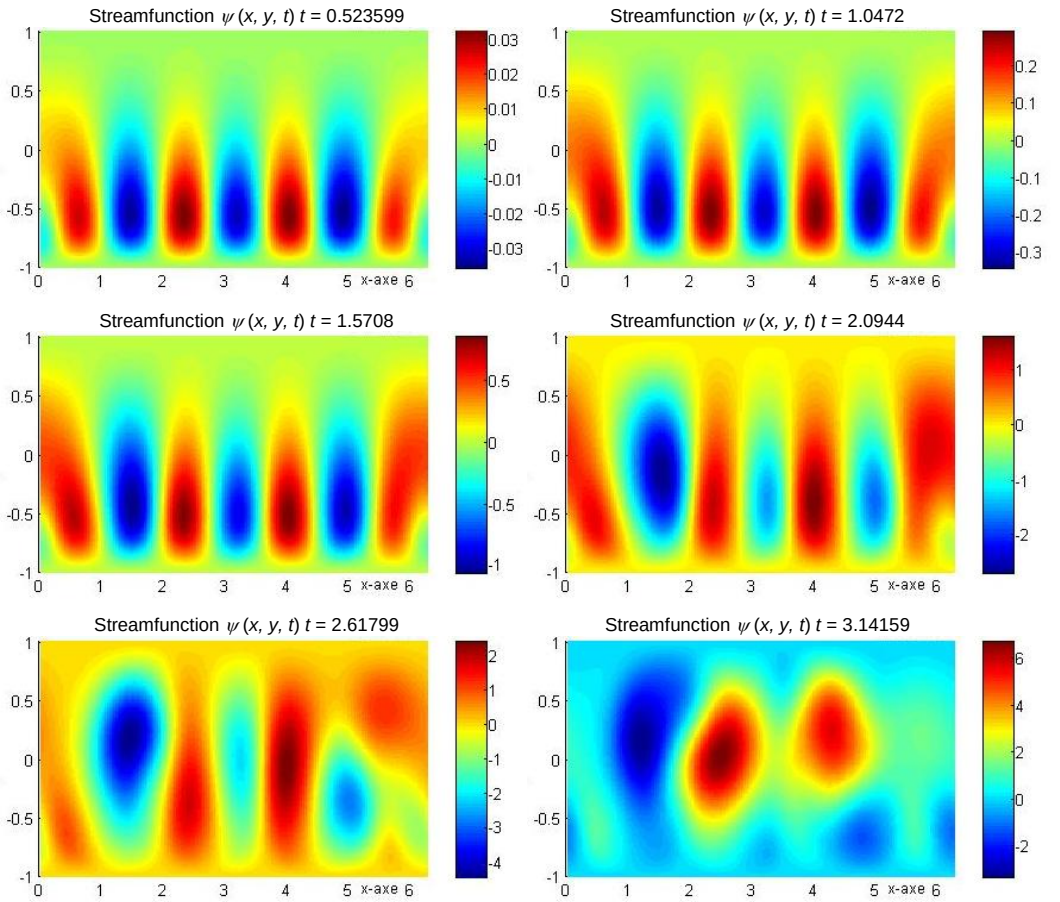

Figure 2. Non-dimensional streamfunction evolution in forced Rayleigh-Benard convection

The lower wall with its temperature modulation is the source of momentum in the initial stages and later the extreme values are shifted in the middle of the channel. The values near the lower wall are increased until $t = 2\pi/3$, and in the next period remain approximatly the same as in the previous instant of time. In this period of time the lower wall serves as the source of momentum in x-direction and feeds the momentum in the middle of the channel.

The v-velocity evolution for the time period $0 \leq t \leq \pi$ is shown in the fig. 4. We can see that the values of v-velocity increase until $t = 5\pi/6$, and later its value fluctuate about the mean value. In fig. 4 we can see the upflow and downflow for $t \geq \pi/2$ at the center of the channel are disturbed. In this case both buoyancy and shear have a destabilizing effect on the flow pattern, and travelling rolls are possible flow structures at $t \geq \pi/2$.

The disturbance in spatial distribution can be seen at $t = 5\pi/6$ and $t = \pi$. We can see that the convection is unavoidable for this Rayleigh number Ra = 1000, for $\delta_m = 0.01$ (forced RBC flow) for each instant of time in the form of forced rolls with the wavenumber $q_m = 3.7$ as can be seen in fig. 4. Only for q_m in the vicinity of the critical wave number q_c the forced rolls remain stable up to fairly large $Ra > Ra_c$. In our case this roll has lost its stability at $t \geq \pi/2$, in spite of the fact that our $q_m = 3.7$ is in the vicinity of the critical wavenumber, and the Rayleigh number Ra = 1000 is significantly below the critical value $Ra_c = 1708$.

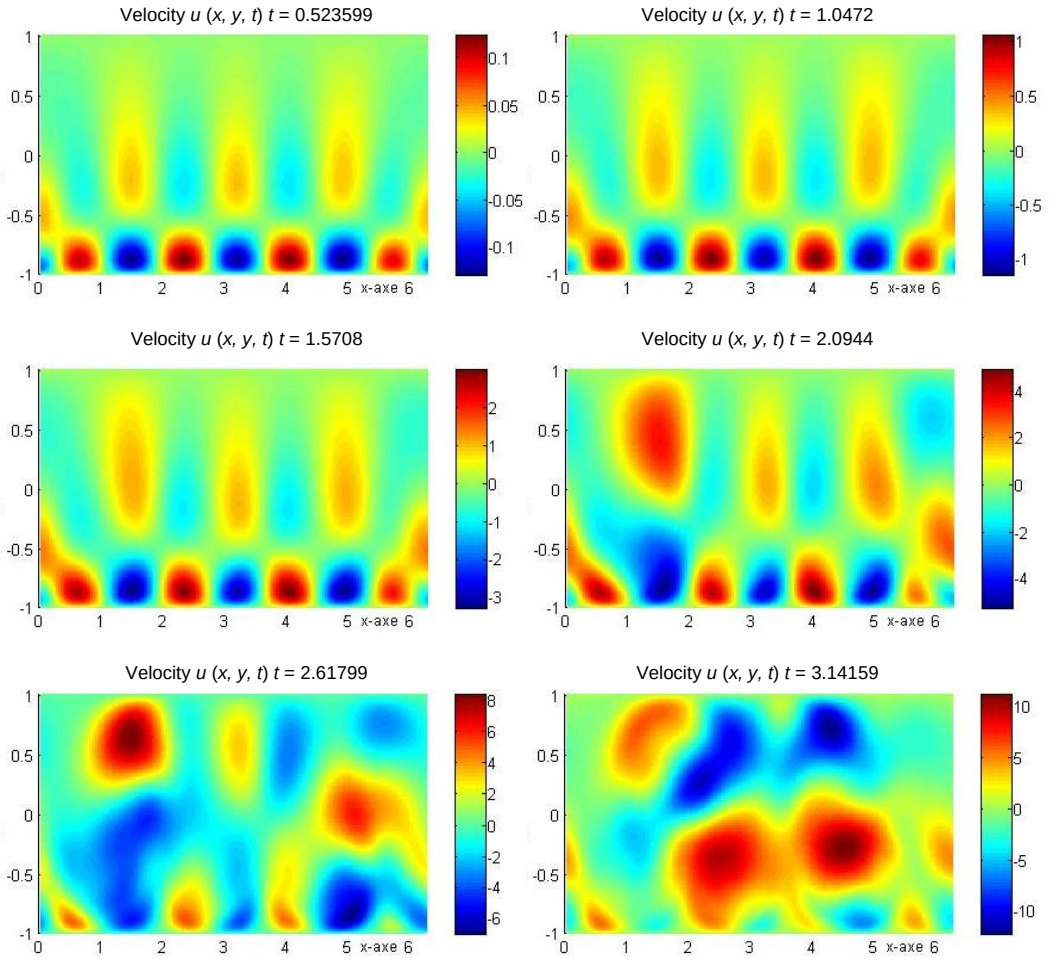

Figure 3. Non-dimensional *u*-velocity evolution in forced Rayleigh-Benard convection

In our simulation the instability is reached at lower values of Ra at the value of wavenumber which is close to the critical one. We have $\mathrm{Ra} < \mathrm{Ra}_c$ but the periodic roll solution exist, since we have $\delta_m \neq 0$. For $\delta_m = 0$ the periodic roll solution can exist only if $\mathrm{Ra} > \mathrm{Ra}_c$. Exploring the stability regime of rolls is a demanding task, and even more difficult is the pattern selection, *i. e*. to understate which is spontaneously chosen by system dynamics.

The compression of the rolls in the interior, which accompanies the enhanced rolls curvature, causes the wavenumber in the cell center to exceed the instability boundary and leads to the formation of the dislocation pairs. These defects then travel toward the wall by climbing in direction normal to the roll axes. The result of this process is the reduction of q_m to the values less than q_c and thus the re-stabilization of the pattern. However the domain walls emit new rolls, which gradually re-compress the ones in the center and thus lead to persistent time dependence.

Above the onset of time dependence, the simulation has shown that the process can be chaotic or periodic apparently depending sensitively on Pr, q_m, and δ_m.

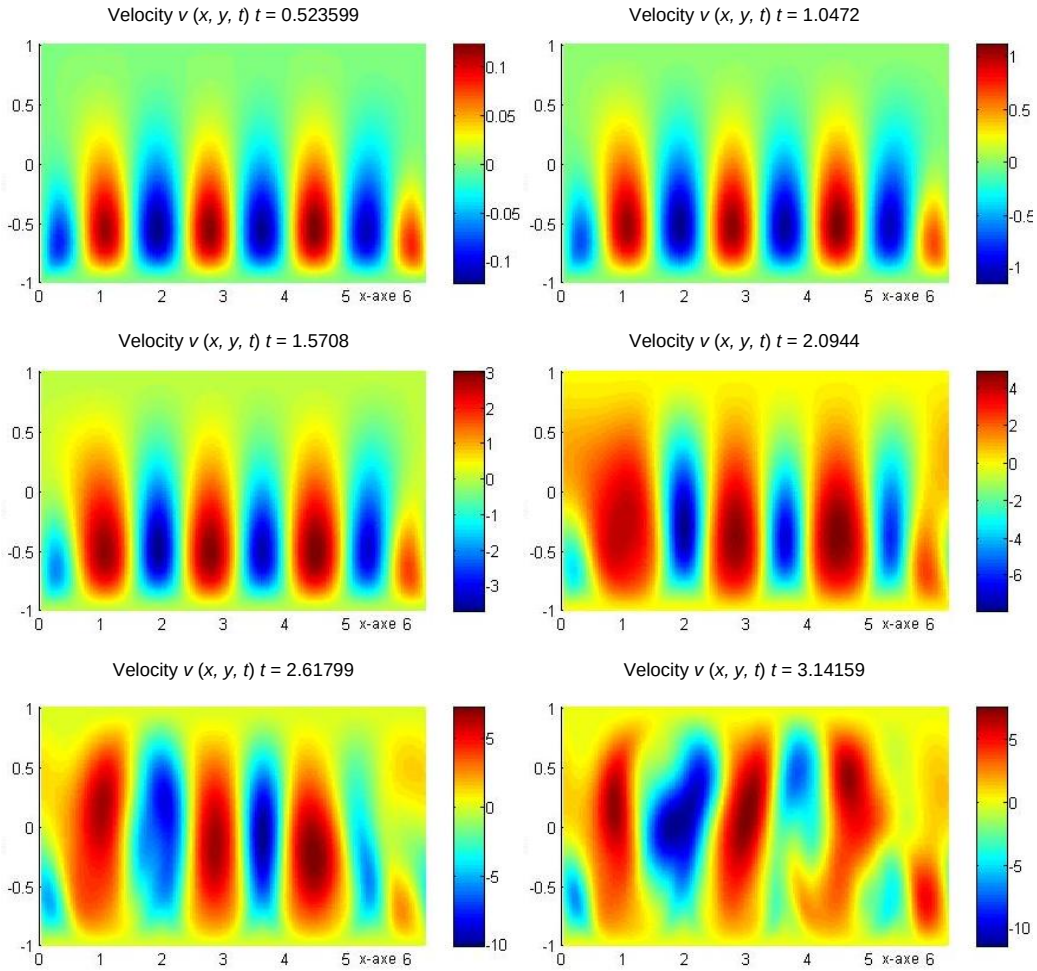

Figure 4. Non-dimensional *v*-velocity evolution in forced Rayleigh-Benard convection

Conclusions

In this paper, we have investigated the FRBC, where, in addition to applied temperature gradient, a sinusoidal temperature modulation with amplitude δ_m and wavenumber q_m is applied at the lower plate. While in unforced RBC the heat conduction state becomes unstable at the critical Rayleigh number Ra_c against convection rolls with wavenumber q_c, forced roll solutions with wavenumber q_m exist at any given Ra.

Various destabilization mechanism acting on forced rolls depend sensitively on the ratio q_m/q_c, and here the results of simulation when this ratio is 1.2 are shown. First we plan to address additional spatial forcing at the upper plate. This opens up new possibilities, in particular when the system is exposed to the presence of non-equal forcing wavenumbers imposed at the two confining plates. Of particular interest is the case of RBC in an inclined fluid layer in the presence of spatial temperatur modulation.

Nomenclature

$\hat{B}_{1,k}(t,y)$ – Fourier coefficient for the convective term $u(\partial\omega/\partial x)$, [–]
$\hat{B}_{2,k}(t,y)$ – Fourier coefficient for the convective term $v(\partial\omega/\partial y)$, [–]
d – distance between plates, [m]
g – gravitational acceleration, [ms^{-2}]
H – half height between plates, [m]
q_m – dimensionless temperature modulation wavenumber, [–]
q_c – critical Rayleigh wavenumber, [–]
Pr – Prandtl number, [–]
Ra – Rayleigh number, [–]
Ra_c – critical Rayleigh number, [–]
$S(x, y, t)$ – dimensionless heat source/sink, [–]
$\hat{s}(t,y)$ – Fourier coefficient for the heat source or heat sink, [–]
$T_1(x, -1, t)$ – temperature of the lower wall, [K]
$T_2(y = 1)$ – temperature of the upper wall, [K]
$T(x, y, t)$ – temperature of the fluid, [K]
t – non-dimensional time, [–]
$u(x, y, t)$ – dimensionless longitudinal velocity component, [–]
$\hat{u}(t,y)$ – Fourier coefficient for u-velocity, [–]
$\bar{v}(x,y,t)$ – dimensionless fluid velocity vector having components (u, v), [–]
$v(x, y, t)$ – dimensionless transversal velocity component, [–]
$\hat{v}(t,y)$ – Fourier coefficient for v-velocity, [–]

Greek symbols

$\alpha(T)$ – thermal diffusivity, [m^{2}s^{-1}]
$\beta(T)$ – thermal expansion coefficient, [K^{-1}]
δ_m – non-dimensional temperature modulation amplitude, [–]
$\delta_{i,j}$ – Kronecker delta, if $i = j$ it is one, otherwise $i \neq j$ it is zero, [–]
$\nu(T)$ – kinematic viscosity, [m^{2}s^{-1}]
$\theta(x, y, t)$ – dimensionless fluid termperature, [–]
$\rho(T)$ – fluid density, [kgm^{-3}]
ω – non-dimensional frequency [–]
$\omega(x, y, t)$ – dimensionless vorticity, [–]
$\psi(x, y, t)$ – dimensionless stream function, [–]

Subscripts

k – Fourier coefficient wavenumber
m – temperatrue modulation
c – critical value
0 – Chebyshev collocation point on the lower wall
N – Chebyshev collocation point on the upper wall

References

[1] Tippelskirch, H., About Convection Cells, Specially in Liquid Sulfur (in German), *Beitr. Phys. Atmos*., 29 (1956), pp. 37-54
[2] Paolucci, S., Chenoweth, D. R., Departures from the Boussinesq Approximation in the Laminar Benard Convection, *Physics of Fluids*, *30* (1987), 5, pp. 1561-1564
[3] Somerscales, E. F. C., Dougherty, T. S., Observed Flow Patterns at the Initiation of Convection in a Horizontal Liquid Layer Heated from Below, *Journal of Fluid Mechanics*, *42* (1970), 4, pp. 755-768
[4] Richter, F. M., Experiments on the Stability of Convection Rolls in Fluids Whose Viscosity Depends on Temperature, *Journal of Fluid Mechanics*, *89* (1978), 3, pp. 553-560
[5] Stengel, K. C., Oliver, D. S., Booker, J. R. Onset of Convection in a Variable-Viscosity Fluid, *Journal of Fluid Mechanics*, *120* (1982), pp. 411-431
[6] Busse, F. H., Frick, H. Square-Pattern Convection in Fluids with Strongly Temperature-Dependent Viscosity, *Journal of Fluid Mechanics*, *150* (1985), pp. 451-465
[7] Severin, J., Herwig, H., Onset of Convection in Rayleigh-Benard Flow with Temperature-Dependent Viscosity: an Asymptotic Approach, ZAMP, *50* (1999), 3, pp. 375-386
[8] Frohlich, J., Laure, P., Peyret, R., Large Departures from Boussinesq Approximation in the Rayleigh-Benard Problem, *Physics of Fluids A, 4* (1992), 7, pp. 1355-1372
[9] Severin, J., Herwig, H., Onset of Convection in the Rayleigh-Benard Flow under Non-Boussinesq Conditions: an Asymptotic Approach, *Forschung im Ingenieurwesen*, *66* (2001), 4, pp. 185-191
[10] Nourollahi, M., Farhadi, M., Kurosh, S., Numerical Study of Mixed Convection and Entropy Generation in the Poiseuille-Benard Channel in Different Angles, *Thermal Science*, *14* (2010), 2, pp. 329-340
[11] Gupta, U., Argawall, U.,Thermal Instability of Compressible Walters' (B-Model) Fluid in the Presence of Hall Currents and Suspended Particles, *Thermal Science*, *15* (2011), 2, pp. 487-500
[12] Kleiser, L., Schumann, U., Treatment of Incompressibility and Boundary Conditions in 3D Numerical Spectral Simulation of Plane Channel Flows, (Ed. E. H. Hirschel), *Proceedings*, Third GAMM Conference Numerical Methods in Fluid Dynamics, 1980, Vieweg, Braunschweig, Germany, pp. 165-173

[13] Pulicani, J. P., A Spectral Multi-Domain Method for the Solution of 1-D Helmholtz and Stokes-Type Equations, *Computers and Fluids*, *16* (1988), 2, pp. 207-215
[14] Jovanovic, M., Simulation of Temporal Hydrodynamic Instability in Plane Channel Flow, *Proceedings*, 2nd *International Congress of Serbian Society of Mechanics (IConSSM)*, Palic, Subotica, Serbia, 2009, B09-B23
[15] Canuto, C. *et al.*, Spectral Methods. Fundamentals in Single Domain, Springer Verlag, 2007
[16] Clever, R. M., Busse, F. H., Transition to Time Dependant Convection, *Journal of Fluid Mechanics*, *65* (1974), 4, pp. 625-645
[17] Busse, F. H., Clever, R. M., Instability of Convection Rolls in a Fluid of Moderate Prandtl Number, *Journal of Fluid Mechanics*, *91* (1979), 2, pp. 319-335

Paper submitted: May 5, 2012
Paper revised: September 20, 2012
Paper accepted: September 25, 2012